Research Square

Preprints are preliminary reports that have not undergone peer review.
They should not be considered conclusive, used to inform clinical practice,
or referenced by the media as validated information.

Magnetic Resonance Imaging Features Differentiate Histologic and Molecular Subtypes of Glioblastoma IDH-Wild Type CNS WHO Grade 4

Sohil H. Patel

spatel63@iuhealth.org

Indiana University Health

Shanna Mayorov

University of Virginia Health System

Wooil Kim

University of Virginia Health System

Kanwar Singh

New York University School of Medicine

James R. Loftus

New York University School of Medicine

James T. Patrie

University of Virginia Health System

Prem P. Batchala

University of Virginia Health System

Allen Ko

University of Virginia Health System

Matthew D. Lee

New York University School of Medicine

Rajan Jain

New York University School of Medicine

David Schiff

University of Virginia Health System

Research Article

Keywords:

Posted Date: December 12th, 2025

DOI: https://doi.org/10.21203/rs.3.rs-8290983/v1

License: This work is licensed under a Creative Commons Attribution 4.0 International License.
Read Full License

Additional Declarations: No competing interests reported.

Version of Record: A version of this preprint was published at Journal of Neuro-Oncology on January 21st, 2026. See the published version at https://doi.org/10.1007/s11060-026-05431-8.

Abstract

Purpose

Glioblastoma IDH-wild type, CNS WHO grade 4 (GBM) can be diagnosed on the basis of histologic features (histological-GBM) or molecular features (molecular-GBM). Only few studies report neuroimaging features of GBM in its modern classification, and none have controlled for surgical status or used multiple logistic regression analysis to determine unique predictors. Our study aimed to validate MRI features that distinguish histological-GBM and molecular-GBM.

Methods

We analyzed a training cohort (n = 255) and validation cohort (n = 44) of GBM cases, classified according to the 2021 WHO Classification of Tumors of the CNS. For the training cohort, univariate and multiple logistic regression analyses determined if MRI metrics (contrast enhancement, ring-enhancement, vasogenic edema, multifocal tumor, lesion diameter, hemorrhage, number of lobes, and normalized ADC) and surgery type (biopsy vs resection) predicted GBM-type (histological vs molecular). A reduced multiple logistic regression model was constructed and applied to the validation dataset.

Results

There were 231 histological-GBMs and 24 molecular-GBMs in the training cohort. Multiple logistic regression analysis including both MRI metrics and surgery type showed that contrast enhancement (OR 7.83 [95%CI: 1.23–49.68], p = 0.029), ring enhancement (OR 5.98 [95%CI: 1.09–32.93, p = 0.040), and normalized ADC (OR 0.78 [95%CI: 0.62–0.99], p = 0.039) differed between histological and molecular-GBM. Analysis of the validation dataset using the unique training dataset-derived predictor variables (contrast-enhancement, ring-enhancement, and normalized ADC) found perfect discrimination between histological and molecular-GBM.

Conclusion

Molecular and histological-GBM exhibit distinct MRI phenotypes independent of surgical status.

INTRODUCTION

In 2016, the World Health Organization (WHO) recognized three categories of adult IDH-wild type (IDH-wt) diffusely infiltrative astrocytomas. These were 1) Diffuse astrocytoma, IDH-wt, WHO grade II; 2) Anaplastic astrocytoma, IDH-wt, WHO grade III; 3) Glioblastoma (GBM), IDH-wt, WHO grade IV [1]. However, it was known that the majority of “lower grade” (i.e. WHO grade II and III) IDH-wt diffuse astrocytomas behaved in a similar manner to GBM IDH-wt WHO grade IV [2]. Furthermore, such lower

grade tumors, while lacking necrosis or microvascular proliferation, harbored molecular features consistent with GBM, including TERT promotor mutation, EGFR amplification, and/or a combined chromosome 7 gain and chromosome 10 loss (+ 7/-10) [2]. As such, in the 2021 (and current) WHO classification of CNS tumors, the diagnosis “Glioblastoma, IDH-wild type, CNS-WHO grade 4” includes diffusely infiltrative astrocytic neoplasms lacking an IDH mutation that have either 1) histologic evidence of necrosis or microvascular proliferation, or 2) any of the following molecular alterations: TERT promotor mutation, EGFR amplification, or combined chromosome + 7/-10 [3].

The neuroimaging correlates of histologically confirmed GBM have been well characterized [4]. However, only few studies have reported GBM neuroimaging features in the context of the updated WHO 2021 classification, where the diagnosis of GBM IDH-wt can be determined with histological criteria (histological-GBM) or molecular criteria (molecular-GBM) [5–8]. Among these studies, none have accounted for the potential confounder of surgery type (biopsy versus resection) in determining whether their GBM cases were classified on the basis of histological or molecular features. In this study, we attempt to address this knowledge gap by analyzing a training cohort and validation cohort of GBM IDH-wt classified according to the 2021 WHO scheme. Our aim was to determine whether MRI features and/or surgery status differed between histological-GBM and molecular-GBM.

METHODS

This retrospective study evaluated MRI metrics and clinical information associated with histological-GBM vs molecular-GBM using training and validation cohorts from our institutions. Institutional Review Board (IRB) approval was obtained for this HIPAA-compliant study.

Patient selection

The training cohort was selected from a neuropathology database at University of Virginia Health containing 262 consecutive GBM IDH-wt cases diagnosed between 2018 and 2023. Inclusion criteria consisted of 1) a pathologic diagnosis of GBM IDH-wt rendered according to the diagnostic criteria of the WHO 2021 classification system; 2) pre-operative MRI with the minimum following pulse sequences: T2*WI/SWI, T2WI/FLAIR, DWI, pre-contrast T1WI, post-contrast T1WI. A total of 7 cases from the training cohort institution were excluded due to lack of minimum required pre-operative MRI data. Of the 255 GBM IDH-wt cases in the training cohort, there were 231 histological-GBMs and 24 molecular-GBMs. A validation cohort of 44 GBM cases (12 molecular-GBMs, 32 age-matched histological-GBMs) was selected from a GBM registry at New York University Medical Center. Demographic data, surgical status (biopsy versus resection), histopathology, and molecular data were all obtained from the electronic medical record. Relevant histological and molecular testing (IDH mutation, TERT promoter mutation, EGFR amplification, Chromosome + 7/-10) was performed according to standard clinical protocol and meeting the WHO 2021 criteria in our Clinical Laboratory Improvement Amendments certified neuropathology laboratories. Histological-GBMs in our cohorts had histological evidence of microvascular proliferation and/or necrosis. Molecular-GBMs in our cohorts lacked histological evidence

of microvascular proliferation or necrosis, but had at least one of the following molecular markers: TERT promoter mutation, EGFR amplification, Chromosome + 7/-10.

Neuroimaging analysis

For the training cohort, pre-operative MRI scans were analyzed in consensus by two board-certified neuroradiologists with 4 and 12 years of experience, respectively, in a blinded fashion. Reproducible-neuroimaging metrics were adopted from prior publications [9, 10], and determined in consensus by the neuroradiologist readers. For each case, readers determined 1) presence/absence of contrast enhancement; 2) presence/absence of ring enhancement; 3) presence/absence of vasogenic edema; 4) presence/absence of multifocal disease; 5) size of whole tumor (long axis diameter, cm); 6) presence/absence of hemorrhage; 8) number of lobes involved; 9) normalized ADC (minimum lesional ADC divided by ADC of normal appearing contralateral white matter, excluding hemorrhage).

Subsequently, an independent board-certified neuroradiologist with 2 years of experience analyzed the MRI scans of the validation cohort in a blinded fashion, recording those MRI metrics that were unique predictors of GBM-type based on the multivariate analysis of the training dataset.

Statistical Analysis

Training dataset analysis:

In the training dataset analysis, univariate and multiple logistic regression was conducted to assess unadjusted and adjusted associations, respectively, between the a-priori selected set of MRI predictors/surgical status and GBM type (histological-GBM, molecular-GBM). Univariate bivariate associations and multivariate adjusted bivariate associations were identified via Wald chi-square tests.

A reduced multiple logistic regression model was then constructed in which the predictors of GBM type were the set of multiple logistic regression predictors identified in step 1 as uniquely associated with GBM type at the 0.05 significance level. Based on the reduced multiple logistic regression model predicted probabilities for histological-GBM, a receiver operating characteristic (ROC) analysis was conducted to identify the optimum predicted probability cut-point (p*) for correctly classifying the training dataset patients as either a histological-GBM or a molecular-GBM. The optimum classification predicted probability cut-point (p*) was identified via the Youden J statistic, where the Youden J statistic = *classification sensitivity* + *classification specificity* – 1 [11].

Validation dataset analyses

Utilizing the training set reduced multiple logistic regression model regression coefficients, predicted probabilities for the histological-GBM were obtained for the validation dataset patients by inserting validation dataset values of the predictors of the reduced multiple logistic regression model into the

reduced multiple logistic regression equation and converting the resulting predicted log-odds values (i.e., ln(θ)) to the probability (p) scale (i.e., $p = e^{\ln(\theta)}/1 + e^{\ln(\theta}$). Based on the validation dataset patients predicted probabilities for histological-GBM, patients were classified as either histological-GBM or molecular-GBM based on whether the patients predicted probability was less than, or greater or equal to p* established in the training dataset analysis. Diagnostic performance was assessed via sensitivity, specificity, positive predictive value (PPV), negative predictive value (NPV), false positive error rate (FPER), false negative error rate (FNER) and accuracy (A). Confidence interval construction for the diagnostic performance measures was based on the binomial-exact method of Agresti et al [12].

RESULTS

Training dataset analysis:

Among the 255 GBM cases in the training dataset, there were 231 histological-GBMs and 24 molecular-GBMs. There were 108 females (42.4%) and 147 males (57.6%). Median age was 65.0 years (interquartile range [IQR]: 58.0–72.0). There was no significant difference in age or gender between molecular-GBM and histological-GBM. Among the histological-GBMs, necrosis was found in 90% of pathological samples, and microvascular proliferation was found in 97.8% of pathological samples. Among the molecular-GBMs, 21 were found to have a TERT promoter mutation, 5 were found to have EGFR amplification, and 7 were found to have chromosome + 7/-10. There were 7 molecular-GBMs that were discovered to have more than one of these molecular alterations. 163 patients underwent surgical resection and 92 patients underwent biopsy. Figures 1 and 2 are representative cases of molecular and histological-GBM, respectively.

Tabulated data and univariate logistic regression associations between GBM type and MRI metrics and surgery type are displayed in Table 1. Histological-GBM was positively associated with the presence of contrast enhancement, ring enhancement, vasogenic edema, and hemorrhage as well as lower normalized ADC ($p < 0.001$, all). Surgical biopsy was associated with molecular-GBM ($p < 0.001$).

Table 1
Tabulated data and univariate associations between MRI metrics/surgical status and GBM type in the training cohort. *Median and interquartile range.

	Histological GBM	Molecular GBM	P-value
Predictor variable			
Contrast enhancement	Present: 227 (93.8%) Absent: 4 (1.7%)	Present: 9 (37.5%) Absent: 15 (62.5%)	**< 0.001**
Ring enhancement	Present: 188 (81.4%) Absent: 43 (18.6%)	Present: 3 (12.5%) Absent: 21 (87.5%)	**< 0.001**
Vasogenic edema	Present: 227 (98.3%) Absent: 4 (1.7%)	Present: 19 (79.2%) Absent: 5 (20.8%)	**< 0.001**
Multifocal	Present: 46 (19.9%) Absent: 185 (80.1%)	Present: 6 (25.0%) Absent: 18 (75.0%)	0.557
Maximum lesional diameter (cm)*	7.3 [5.3, 9.2]	6.35 [5.1, 7.3]	0.127
Hemorrhage	Present: 195 (84.4%) Absent: 36 (15.6%)	Present: 6 (25.0%) Absent: 18 (75.0%)	**< 0.001**
Number of lobes involved*	2 [2, 3]	2.5 [2, 3]	0.392
Normalized ADC*	0.83 [0.72, 0.95]	1.23 [0.92, 1.49]	**< 0.001**
Surgery type	Resection: 157 (68.0%) Biopsy: 74 (32.0%)	Resection: 6 (25.0%) Biopsy: 18 (75.0%)	**< 0.001**

Multiple logistic regression analysis revealed significant information about GBM type explained by the regression model (Wald $X^2 = 39.59$, $p < 0.001$), with a model C-statistic of 0.91 (95% CI: [0.83, 0.99]). Adjusted odds ratios (AOR) for quantifying the association between GBM type and the MRI metrics and surgical type are displayed in Table 2. Contrast enhancement was positively associated with histological-GBM (AOR 7.83; 95% CI: [1.23, 49.68], p = 0.029). Ring enhancement was positively associated with histological-GBM (AOR 5.98; 95% CI: [1.09, 32.93], p = 0.040). Normalized ADC was negatively associated with histological-GBM (AOR 0.78; 95% CI [0.62, 0.99], p = 0.039). Vasogenic edema, hemorrhage, and surgery type were not uniquely associated with GBM type in the multiple logistic regression setting.

Table 2
Multivariate exact logistic regression adjusted odds ratios for quantifying the association between the MRI metrics/surgical status and GBM type in the training cohort (0 = Molecular-GBM, 1 = Histological-GBM).

Predictor variable	Ratio	Odd Ratio [95% CI]	P-value
Contrast enhancement	Present: Absent	7.83 [1.23, 49.68]	**0.029**
Ring enhancement	Present: Absent	5.98 [1.09, 32.93]	**0.040**
Vasogenic edema	Present: Absent	3.32 [0.33, 33.69]	0.310
Multifocal	Present: Absent	1.63 [0.22, 12.30]	0.635
Maximum tumor diameter	X + 1:X	0.93 [0.67, 1.30]	0.678
Hemorrhage	Present: Absent	2.90 [0.62, 13.42]	0.174
Number of lobes involved	X + 1:X	0.50 [0.24, 1.05]	0.066
Normalized ADC	X + 0.1:X	0.78 [0.62, 0.99]	**0.039**
Surgery type	Resection:Biopsy	2.36 [0.55, 10.22]	0.250

As the final step in the training dataset analysis, a reduced multiple logistic regression model was constructed to predict GBM type utilizing only the predictor variables in Table 2 that were uniquely associated with GBM type (contrast enhancement, ring enhancement, and normalized ADC). ROC analysis established an optimum diagnostic classification probability threshold of 0.85, where a predicted probability of ≥ 0.85 was classified as histological-GBM, and a predicted probability of < 0.85 was classified as molecular-GBM. When this classification rule was applied to the 231 histological-GBM training dataset patients, 222 patients (96.1%) were correctly classified as histological-GBM. When this classification rule was applied to the 24 molecular-GBM training dataset patients, 18 patients (75.0%) were correctly classified as molecular-GBM.

Validation dataset analysis:

Among the 44 GBM cases in the validation dataset, there were 32 histological-GBMs and 12 molecular-GBMs. There were 16 females (36.4%) and 28 males (64.6%). Median age was 63.0 years (interquartile range [IQR]: 52.5–71.0). There was no significant difference in age or gender between molecular-GBM and histological-GBM.

Predicted probabilities for histological-GBM were obtained for the validation dataset cases by inserting the validation dataset information for contrast enhancement, ring enhancement, and normalized ADC into the training dataset derived reduced multiple logistic regression model equation and converting the resulting predicted log-odds values (i.e., ln(θ)) to the probability (p) scale (i.e., $p = e^{\ln(\theta)}/1 + e^{\ln(\theta}$).

Validation dataset patients whose predicted probability was ≥ 0.85 were classified as histological-GBM and validation dataset patients whose predicted probability was < 0.85 were classified as molecular-GBM. Validation diagnostic performance is summarized by traditional measures of diagnostic performance in Table 3. Application of the aforementioned diagnostic classification rule resulted in correct classification of all 32 histological-GBMs and all 12 molecular-GBMs in the validation dataset.

Table 3
Validation diagnostic performance measures, with respect to classifying GBM type (histological-GBM versus molecular-GBM) when the training set reduced multiple logistic regression model coefficients were applied to contrast enhancement, ring enhancement, and normalized ADC data of the validation dataset. GBM type classification was based on an optimum probability (p*=0.85) threshold established based on the training dataset patients. Validation dataset patients who had a predicted probability ≥ 0.85 were classified as histological-GBM patients and validation dataset patients who had a predicted probability is < 0.85 were classified as molecular-GBM.

Diagnostic Performance Measure	Measure Value (%) [95% CI]
Sensitivity	100 [89.1, 100]
Specificity	100 [73.5, 100]
Positive Predictive Value (PPV)	100 [89.1, 100]
Negative Predictive Value (NPV)	100 [73.5, 100]
False Positive Error Rate (FPER)	0.00 [0.00. 26.5]
False Negative Error Rate (FNER)	0.00 [0.00, 10.9]
Accuracy	100 [92.0, 100]

DISCUSSION

The pathologic diagnosis of GBM has undergone significant revision in the prior decade with the incorporation by the World Health Organization of molecular markers into its diagnostic criteria. Prior to 2016, GBM was diagnosed based entirely on histologic criteria, namely the presence of a diffusely infiltrating astrocytic neoplasm with either necrosis or microvascular proliferation [13]. On the basis of a histologically-based diagnostic standard, MRI features of glioblastoma were established, including contrast enhancement, ring enhancement, low ADC values, increased cerebral blood volume, and elevated choline levels, among other metrics [14–17].

However, it was long known that some so-called “lower grade” gliomas behaved in an aggressive fashion, similar to GBMs [18–19]. An initial step towards resolving this issue was taken by the WHO in 2016, when IDH mutation status was incorporated into the classification scheme of diffuse gliomas [1]. Diffuse gliomas with IDH-wt status were recognized as generally more aggressive than their IDH-mutant counterparts. Further diagnostic specificity was established in the WHO 2021 classification scheme,

where the diagnosis of glioblastoma could be established in an IDH-wt diffuse astrocytic neoplasm either on basis of histologic features (microvascular proliferation and/or necrosis) or molecular features (TERTp mutation, EGFR amplification, or chromosome + 7/-10) [3]. The current diagnostic category of GBM is different than in the past, when nearly all radiologic studies were performed establishing the MRI appearance of glioblastoma. The current diagnostic category of Glioblastoma, IDH-wild type, CNS-WHO grade 4 contains many tumors that would have been previously classified as WHO grade II or III gliomas due to lack of microvascular proliferation and necrosis. It also no longer includes IDH-mutant gliomas that have microvascular proliferation and/or necrosis, namely most tumors in the current category “Astrocytoma, IDH-mutant, CNS-WHO grade 4” [3].

Our study establishes that, indeed, the majority of GBMs (which continue to be diagnosed on the basis of histologic features alone) demonstrate typical MRI features long associated with glioblastoma, including contrast enhancement, ring enhancement, edema, hemorrhage, and low ADC values relative to normal-appearing white matter. However, there is a significant minority of glioblastomas, namely those diagnosed on the basis of molecular features, that show distinct MRI features not typically associated with GBM. Such tumors often show no contrast enhancement, and have less frequent edema, less frequent hemorrhage, and higher ADC values compared to histologically-diagnosed GBM (Table 1). These results should be instructive to neuroradiologists and other members of neuro-oncology teams in the diagnostic work up of glioma patients. In particular, they support the point, with modern neuropathologic and neuroimaging data, that non-enhancing tumors on MRI should not be reflexively equated with “low grade gliomas” [20].

Our findings support the results of the few relevant studies in the literature. Guo et al [6] investigated a cohort of 191 GBMs, including 146 histological-GBMs and 45 molecular-GBMs. They found that molecular-GBMs (vs histological GBMs) were less likely to have contrast-enhancement (78.8% vs. 95.3%, $p = 0.006$) and intratumoral necrosis (63.6% vs. 85.3%, $p = 0.005$). Foltyn-Dumitru et al [7] investigated 352 GBM IDH-wt and found that non-contrast-enhancing GBM (vs contrast-enhancing GBM) less frequently had microvascular proliferation (39% vs. 94%) and necrosis (25% vs. 92%) ($P < .001$) on pathologic assessment, and were more likely to require molecular criteria for diagnosis ($P < .001$). The relative strengths of our study include inclusion of a much greater number of MRI metrics and the use of multiple logistic regression statistical analysis to determine unique predictors of GBM-type. Furthermore, we validated our results using an independent cohort analyzed by a different neuroradiologist and found perfect classification of glioblastoma type in the validation cohort using our training dataset derived reduced multiple logistic regression model. Unlike prior studies, our study incorporated surgical status in our multivariate analysis. As expected, among glioblastomas in our training cohort, the requirement for molecular testing was more common when a surgical biopsy was performed (Table 1). This could reflect the fact that, with a surgical biopsy, there is greater risk of under-sampling and “missing” a tumoral sample which has necrosis or microvascular proliferation. It might also reflect the fact that diffuse non-enhancing glioblastomas are less optimal surgical targets for therapeutic resection and are thus more likely to be biopsied for diagnostic purposes only [18]. However, despite the strong association between

surgical status and glioblastoma type in the univariate analysis, only MRI metrics remained significant predictors of glioblastoma type in our multivariate analysis.

Our study has limitations. We used a retrospective study design that would benefit from prospective validation. Our validation cohort was comprised of 44 patients, and independent validation with larger cohorts would better establish the predictive value of MRI metrics. While our choice of relatively simply MRI metrics helps ensure straightforward clinical application, it is also possible that advanced MRI techniques (including MR perfusion and MR spectroscopy) and AI-based classification tools could provide valuable insights into glioblastoma phenotypes. Differences in pathologic reporting between the training and validation institutions, including increased sensitivity for microvascular proliferation, could have contributed to better performance of the model in the validation cohort, as this feature is known to correlate with increased probability of enhancement. Finally, we did not distinguish between molecular-GBMs on the basis of histologic features or patient age, factors that have been recently proposed for future GBM classification [21].

CONCLUSION

Our study establishes that molecular-GBMs associate with absent contrast enhancement/ring-enhancement on MRI, and have higher ADC values compared to histological-GBMs. These associations are significant independent of surgical status. Recognition of the phenotypic variability of GBMs is important for neuro-oncology teams in the accurate pre-operative characterization of these lesions.

Declarations

Funding:

None.

Conflicts of interest/Competing interests: The authors declare they have no conflicts of interest.

Ethics approval: Institutional Review Board approval was obtained for this retrospective study.

Consent to Participate: The requirement for informed consent was waived by the Institutional Review Board.

Consent for Publication: The requirement for informed consent was waived by the Institutional Review Board.

Availability of data and material (data transparency): The authors confirm that the data supporting the findings of this study are available within the article and its supplementary materials. If there are requests for additional data, they can be sent to the corresponding author (S.H.P.).

Code availability (software application or custom code): N/A.

Author Contribution

Conception or design of the work: SHP, KS, JDR, MDL, RJ, DSAcquisition and analysis of data: SHP, SM, WK, PPB, AKData Analysis: JTPManuscript drafting and revision: All authors

Data Availability

The authors confirm that the data supporting the findings of this study are available within the article and its supplementary materials. If there are requests for additional data, they can be sent to the corresponding author (S.H.P.).

References

1. Louis DN, Perry A, Reifenberger G et al (2016) The 2016 World Health Organization Classification of Tumors of the Central Nervous System: a summary. Acta Neuropathol 131(6):803–820. 10.1007/s00401-016-1545-1
2. Brat DJ, Aldape K, Colman H et al (2018) cIMPACT-NOW update 3: recommended diagnostic criteria for Diffuse astrocytic glioma, IDH-wildtype, with molecular features of glioblastoma, WHO grade IV. Acta Neuropathol (Berl) 136(5):805–810. 10.1007/s00401-018-1913-0
3. Louis DN, Perry A, Wesseling P et al (2021) The 2021 WHO Classification of Tumors of the Central Nervous System: a summary. Neuro Oncol 2(8):1231–1251
4. Cha S (2006) Update on Brain Tumor Imaging: From Anatomy to Physiology. Am J Neuroradiol 27(3):475–487
5. Lee D, Riestenberg RA, Haskell-Mendoza A, Bloch O (2021) Diffuse astrocytic glioma, IDH-Wildtype, with molecular features of glioblastoma, WHO grade IV: A single-institution case series and review. J Neurooncol 152(1):89–98. 10.1007/s11060-020-03677-4
6. Guo X, Gu L, Li Y et al (2023) Histological and molecular glioblastoma, IDH-wildtype: a real-world landscape using the 2021 WHO classification of central nervous system tumors. Front Oncol 13:1200815. 10.3389/fonc.2023.1200815
7. Foltyn-Dumitru M, Banan R, Schell M et al (2025) Histopathological and molecular characteristics of IDH-wildtype glioblastoma without contrast enhancement: Implications for clinical outcomes. Neuro-Oncol. 10.1093/neuonc/noaf070
8. Agarwal A, Edgar MA, Desai A, Gupta V, Soni N, Bathla G, Molecular (2024) GBM versus Histopathological GBM: Radiology-Pathology-Genetic Correlation and the New WHO 2021 Definition of Glioblastoma. AJNR Am J Neuroradiol 45(8):1006–1012. 10.3174/ajnr.A8225
9. Joyner DA, Garrett J, Batchala PP et al (2023) MRI features predict tumor grade in isocitrate dehydrogenase (IDH)-mutant astrocytoma and oligodendroglioma. Neuroradiology 65:121–129

10. Patel SH, Batchala PP, Muttikkal I et al (2021) Fluid attenuation in non-contrast-enhancing tumor (nCET): an MRI Marker for Isocitrate Dehydrogenase (IDH) mutation in Glioblastoma. J Neurooncol 152:523–531
11. Schisterman EF, Perkins NJ, Liu A, Bondell H (2005) Optimal cut-point and its corresponding Youden Index to discriminate individuals using pooled blood samples. Epidemiology 16(1):73–81
12. Agresti A, Coull BA (1998) Approximate is better than exact for interval estimation of binomial proportions. Am Stat 52:119–126
13. Louis DN, Ohgaki H, Wiestler OD et al (2007) The 2007 WHO classification of tumours of the central nervous system. Acta Neuropathol 114(2):97–109
14. Rees JH, Smirniotopoulos JG, Jones RV, Wong K (1996) Glioblastoma multiforme: radiologic-pathologic correlation. Radiographics 16:1413–1438
15. Knopp EA, Cha S, Johnson G et al (1999) Glial neoplasms: dynamic contrast-enhanced T2*-weighted MR imaging. Radiology 211(3):791–798
16. Kono K, Inoue Y, Nakayama K et al (2001) The Role of Diffusion-weighted Imaging in Patients with Brain Tumors. Am J Neuroradiol 22(6):1081–1088
17. Law M, Cha S, Knopp EA, Johnson G, Arnett J, Litt AW (2002) High-grade gliomas and solitary metastases: differentiation by using perfusion and proton spectroscopic MR imaging. Radiology 222(3):715–721
18. van den Bent MJ, Snijders TJ, Bromberg JE (2012) Current treatment of low grade gliomas. Memo 5(3):223–227
19. Law M, Oh S, Johnson G et al (2006) Perfusion Magnetic Resonance Imaging Predicts Patient Outcome as an Adjunct to Histopathology: A Second Reference Standard in the Surgical and Nonsurgical Treatment of Low-grade Gliomas. Neurosurgery 58:1099–1107
20. Kondziolka D, Lunsford LD, Martinez AJ (1993) Unreliability of contemporary neurodiagnostic imaging in evaluating suspected adult supratentorial (low-grade) astrocytoma. J Neurosurg 4:533–536
21. Wesseling P, Capper D, Reifenberger G et al cIMPACT-NOW update 11: Proposal on adaptation of diagnostic criteria for IDH- and H3-wildtype diffuse high-grade gliomas and for posterior fossa ependymal tumors. Brain Pathol 2025 Aug 31:e70035. 10.1111/bpa.70035

Figures

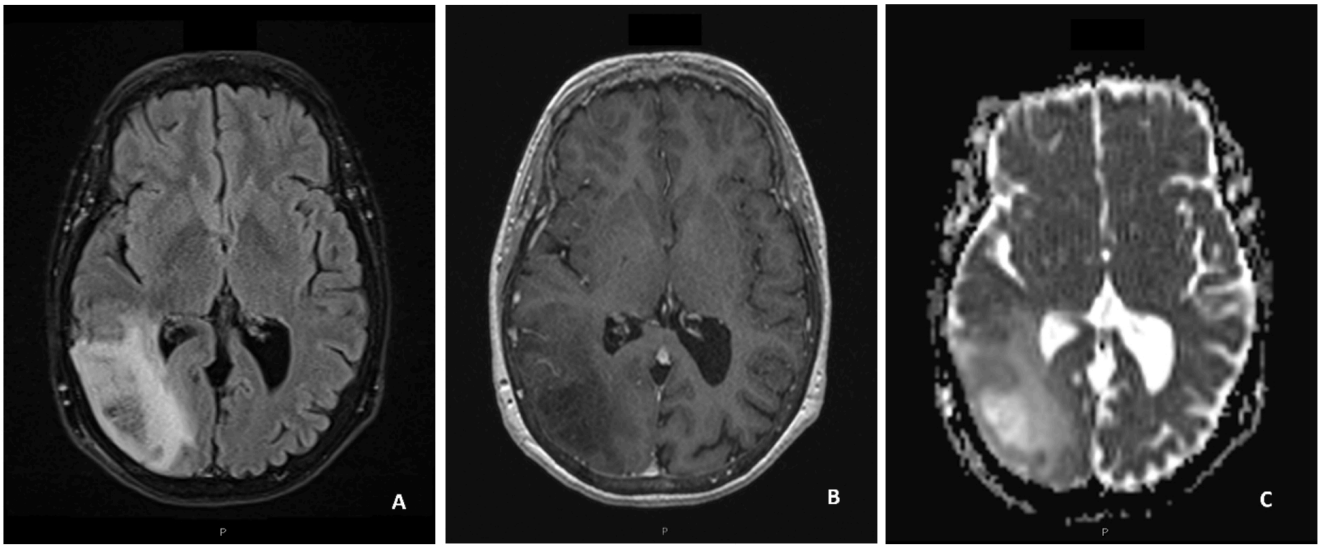


Figure 1

Molecular GBM. 64 year-old female with right temporal-occipital Glioblastoma, IDH-wild type, CNS-WHO grade 4. Histologically, there was no evidence of microvascular proliferation or necrosis. Molecular testing revealed a TERT-promoter C228T mutation and chromosome 7 gain/10 loss. (A) FLAIR sequence shows a predominantly hyperintense infiltrative mass. (B) Contrast-enhanced T1WI shows no contrast enhancement of the mass. (C) ADC map shows predominantly high signal. Minimum normalized ADC was 1.6.

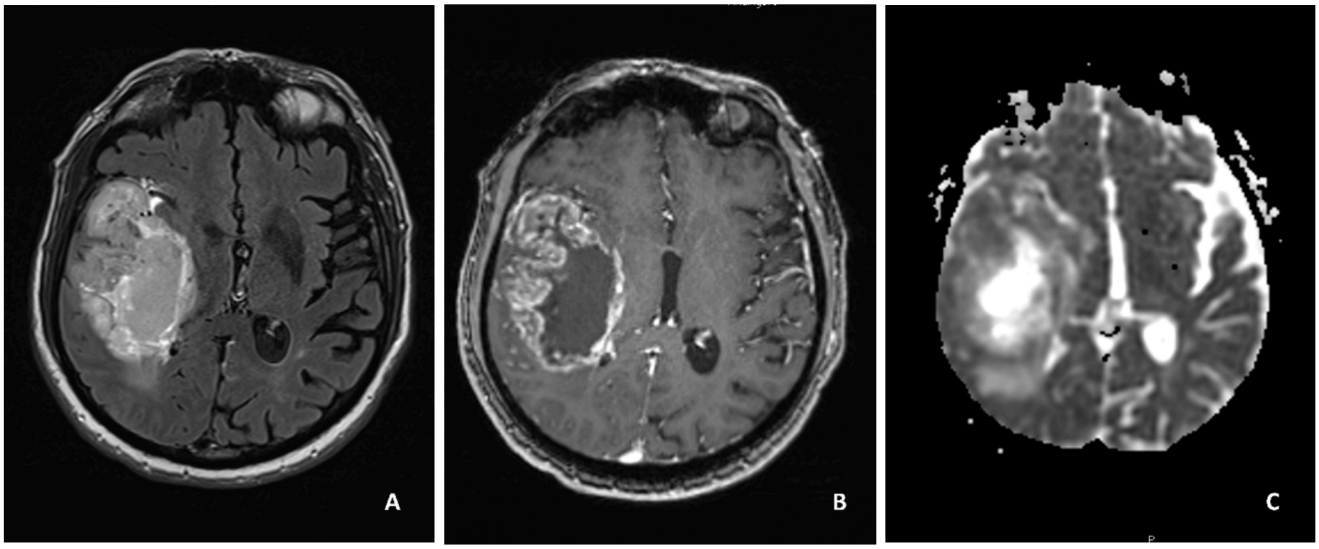


Figure 2

Histological GBM. 70 year old male with right insular-temporal Glioblastoma, IDH-wild type, CNS WHO grade 4. Histological evidence of necrosis and microvascular proliferation was present. (A) FLAIR sequence shows a heterogenous hyperintense mass. (B) Contrast-enhanced T1WI shows marked, thick ring-enhancement surrounding a central necrotic cavity. (C) ADC map shows regions of low signal corresponding to the contrast-enhancing tumor. Minimum normalized ADC was 0.9.